Extremely High Two-Photon Absorbing Graphene Oxide for Imaging of Tumor Cells in the Second Biological Window

ARTICLE *in* JOURNAL OF PHYSICAL CHEMISTRY LETTERS · JUNE 2014

Impact Factor: 7.46 · DOI: 10.1021/jz5009856

6 AUTHORS, INCLUDING:

Avijit Pramanik
Jackson State University
53 PUBLICATIONS **405** CITATIONS

SEE PROFILE

Suhash Chavva
Jackson State University
14 PUBLICATIONS **34** CITATIONS

SEE PROFILE

THE JOURNAL OF PHYSICAL CHEMISTRY Letters

Letter

pubs.acs.org/JPCL

Extremely High Two-Photon Absorbing Graphene Oxide for Imaging of Tumor Cells in the Second Biological Window

Avijit Pramanik, Suhash Reddy Chavva, Zhen Fan, Sudarson Sekhar Sinha, Bhanu Priya Viraka Nellore, and Paresh Chandra Ray*

Department of Chemistry and Biochemistry, Jackson State University, Jackson, Mississippi 39217, United States

ABSTRACT: Cancer, a life-threatening disease, has become a global pandemic. Targeted tumor imaging using near-infrared (NIR) light is the key to improve the penetration depth and it is highly promising for clinical tumor diagnostics. Driven by this need, in this Letter we have reported aptamer conjugated graphene oxide-based two-photon imaging of breast tumor cells selectively. Reported data indicate that there is an extremely high two-photon absorption from aptamer conjugated graphene oxide (σ_{2PA} = 46890 GM). Experimental data show that two-photon luminescence signal remains almost unchanged even after 2 h of illuminations. Reported results show that S6 RNA aptamers conjugated graphene oxide-based two-photon fluorescence can be used for selective two-photon imaging of SK-BR-3 breast tumor cell in second biological transparency windows using 1100 nm wavelength. Experimental data demonstrate that it is highly capable of distinguishing targeted breast cancer SK-BR-3 cells from other nontargeted MDA-MB-231 breast cancer cells.

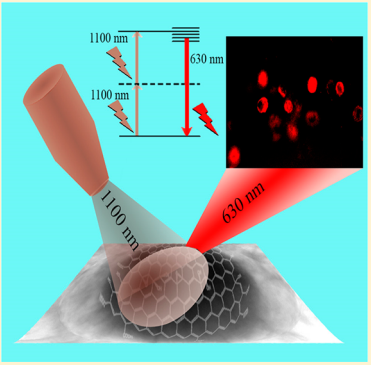

SECTION: Physical Processes in Nanomaterials and Nanostructures

Cancer has been known for more than 3000 years, but still in the 21st century, it is one of the most life-threatening diseases, causing 1 in 8 deaths worldwide.[1−5] Breast cancer is the second leading cause of cancer deaths in women today, after lung cancer.[6−10] Although we all know that early detection is the key for survival, it is still an important challenge for society.[1−10] For in vivo cancer imaging without surgery, near-infrared (NIR) light between 650−950 nm for the first NIR window and 1000−1350 nm for the second NIR window must be used to avoid absorption by physiological fluids.[6−11] Since human blood exhibits transparency from 1000 to 1350 nm, the second window thus provides a maximum radiation penetration through tissue.[12−18] Despite huge advances in organic fluorescence probes in the last several decades, still today the fluorescence imaging using second NIR window light remains a huge challenge.[6−13] Two-photon fluorescence (TPF) imaging has been introduced as an alternative for NIR imaging.[11−18]

TPF has several advantages for tumor imaging and these are larger penetration depth, minimized tissue autofluorescence background, and reduced photodamage.[11−18] The efficiency of TPF imaging is highly dependent on the two-photon absorption cross sections in water and also on long time photostability. However, the rapid photobleaching and low two-photon absorption cross-section (50 Goeppert−Mayer (GM)) use of organic dyes for TPF has been hampered for real-life imaging.[11−18] For a finding better two-photon luminescence imaging platform, the current Letter reports on a water-soluble S6 RNA aptamer-conjugated graphene oxide (GO)-based two-photon photoluminescence probe for targeted bioimaging of SK-BR-3 breast cancer cells in second biological transparency window using 1100 nm wavelength, as shown in Scheme 1. To demonstrate the selectivity, we have used SK-BR-3 and MDA-MB-231, breast cancer cell lines, where the first one is targeted and the second one is nontargeted.

For the past decade, after its discovery in 2004, graphene has revolutionized the scientific community due to its remarkable

Scheme 1. Schematic Representation Showing Aptamer-Bound Graphene Oxide-Based Two-Photon Luminescence Imaging Platform for Selective Cancer Cell Imaging

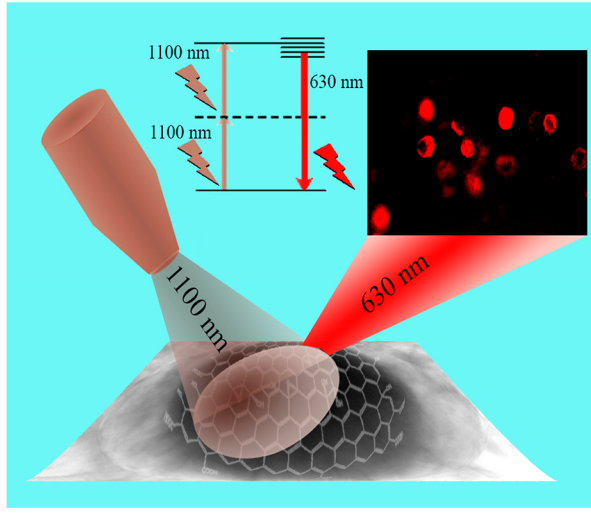

Received: May 17, 2014
Accepted: June 6, 2014

   dx.doi.org/10.1021/jz5009856 | J. Phys. Chem. Lett. 2014, 5, 2150−2154

electronic and structural properties.[19−28] Unfortunately, due to the presence of zero optical band gap, graphene is unable to exhibit good luminescence.[26−33] Recently, several groups have reported that photoluminescence of graphene can be observed by modifying it with various oxygen-containing groups or by reducing its size to the nanometer scale.[34−44] Several reported experimental data demonstrated that GO photoluminescence can be tuned from the visible to the near-NIR region just by varying the excitation energy from 440 to 600 nm.[31−38] Since clear fluorescence cannot be observed above 600 nm excitation, GO is not suitable for biological imaging applications using NIR light within the first and second biological transparency windows. Driven by the need, here we report an extremely high two-photon absorption cross-section from GO and its use for two-photon imaging of breast tumor SK-BR-3 cells for their good biocompatibility and photostability. It is well documented[45] that human epidermal growth factor receptor 2 (HER2)/neu oncogene is overexpressed by SK-BR-3 breast cancer cells.

As a result, for selective imaging of SK-BR-3 cells, we conjugated GO with S6 RNA aptamer, which is known to be specific to bind with SK-BR-3 cell via HER2.[45] Our reported data show that aptamer-conjugated GO is highly capable of distinguishing targeted breast cancer SK-BR-3 cells from other nontargeted MDA-MB-231 breast cancer cells.

We synthesized GO using a modified Hummers method from graphite exfoliation,[24] as we and others have reported earlier.[25−30] For targeted two-photon imaging of SK-BR-3 cancer cells, we modified GO with S6 RNA-aptamer. For this purpose, at first, GO was coated by thiolated HS-PEG. After PEGylation, NH-modified S6 RNA-aptamers were attached with acid chloride-functionalized GO. For two-photon absorption and imaging, we used an 80 MHz Ti-sapphire laser as an excitation source with 100 fs pulse width and 80 MHz repetition rate. 1100 nm light in the second biological transparency windows were generated using an anoptical parametric amplifier. A Nikon multiphoton microscope (FV1000MPE) was used for two-photon imaging. Experimental details have been reported earlier.[11] For the measurement of two-photon absorption, we used two-photon excited fluorescence spectra. TPF spectra were recorded with a charge-coupled device (CCD) camera after passing through a monochromator. As we have discussed before, the two-photon luminescence intensity depends on the two-photon absorption cross-section (σ_{2p}) and the fluorescence quantum yield (Φ_f). For the determination of two-photon cross sections and fluorescence quantum yield, we have used rhodamine B (RhB) as a reference. Two-photon absorption cross-section values were obtained using the following equation:

$$\sigma_{GO} = \sigma_{RhB} \times (F_{GO}/F_{RhB}) \times (\Phi_{RhB}/\Phi_{GO}) \times (C_{RhB}/C_{GO}) \quad (1)$$

where F is the observed fluorescence intensity, the quantum yield is represented by Φ, and C is the concentration. Fluorescence quantum yield of synthesized aptamer-attached GO was determined to be 0.35.

Figure 1A shows the fluorescence properties of aptamer-attached GO. Our experimentally determined spectra clearly indicate that single-photon photoluminescence spectra can be tuned just by varying the excitation energy without changing its chemical composition and size. This excitation energy-dependent photoluminescence spectral shift for aptamer-attached GO can be due to several factors as reported earlier,[30−38] and these

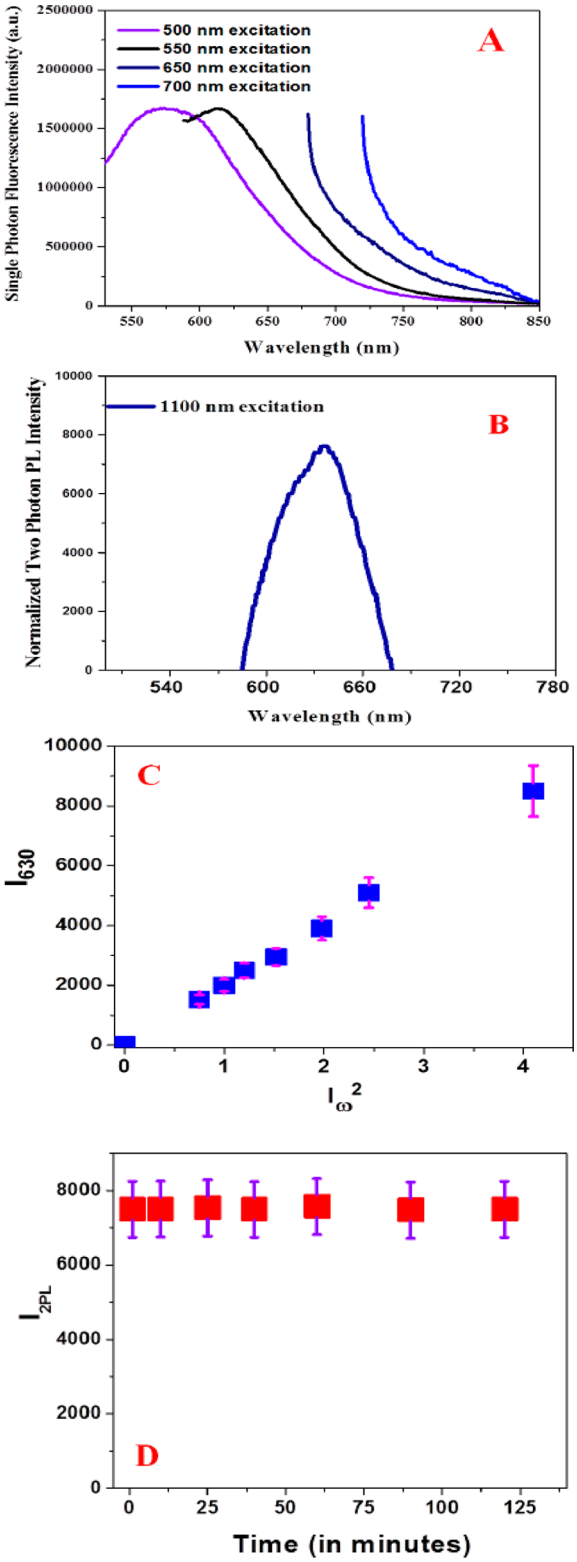

Figure 1. (A) Excitation wavelength-dependent photoluminescence from freshly prepared S6 RNA-attached GO. (B) Two-photon photoluminescence spectrum from freshly prepared S6 RNA-conjugated GO, when aptamer-attached GO was excited using 1100 nm light. (C) Plot demonstrates how the photoluminescence at 630 nm varies with the square of intensity of 1100 nm excitation. (D) Plot shows the photostability of S6 RNA aptamer-conjugated GO.

are (1) excitation wavelength-dependent fluorescence from the −OH, −COOH, and −COOCl moieties in the GO sheets; (2)

dx.doi.org/10.1021/jz5009856 | J. Phys. Chem. Lett. 2014, 5, 2150−2154

the local reorganization of photoexcited GO sheets in a polar solvent. Although the aptamer-conjugated GO photoluminescence can be tuned by varying the excitation energy, we have not observed any clear fluorescence above 550 nm excitation, which clearly indicates that the aptamer conjugated GO is not suitable for biological imaging applications using the biological transparency windows. To overcome this, we used TPF imaging at the second biological transparency window for breast tumor cells imaging. Figure 1B shows two-photon photoluminescence from freshly prepared S6 RNA aptamer-conjugated GO, at 1100 nm excitation. To understand whether the observed luminescence was induced by two-photon excitation, we performed 1100 nm excitation wavelength power-dependent two-photon intensity measurement. Figure 1C shows how 630 nm two-photon emission intensities from GO vary for 1100 nm laser excitation with various average powers. Our reported data indicate that the emission intensity is proportional to the square of the excitation intensity, which confirms the two-photon excitation process. Using eq 1, we found that the two-photon absorption cross-section is 46890 GM, at 1100 nm excitation for −NH-modified S6 RNA aptamer-conjugated GO. On the other hand, the measured σ_{2PA} for RhB was only 28 GM. The measured σ_{2PA} for S6 RNA aptamer conjugated GO is a few orders of magnitude larger than that of organic molecules and even higher than that of the highest reported two-photon absorption cross-section for quantum dots.[20]

Our reported very high σ_{2PA} for S6 RNA aptamer-conjugated GO can be due to highly efficient intramolecular charge transfer between large π-conjugated systems of water-soluble GO and the strong electron donating carboxy, hydroxyl, and amine group. This strong intramolecular charge transfer enhances the two-photon absorption cross-section and, as a result, strong two-photon-induced fluorescence has been observed.

For two-photon imaging, good photostability is one of the strongest criteria material should exhibit. As a result, next we performed the photostability experiment for S6 RNA aptamer-conjugated GO. As shown in Figure 1D, two-photon luminescence signals remain almost unchanged even after 2 h of illuminations, which shows the very good photostability of S6 RNA aptamer-conjugated GO. Due to the extremely high two-photon absorption cross-section and good quantum yield, aptamer-attached GO can be a highly promising two-photon luminescence microscopy imaging contrast agent for cancer imaging. Next, we incubated S6 RNA aptamer-conjugated GO with different concentrations of SK-BR-3 breast cancer cells for 30 min. After that, unconjugated breast cancer cells were separated using centrifugation followed by washing with buffer. We performed this process three times to make sure that the unconjugated SK-BR-3 breast cancer cells were separated nicely from the aptamer-conjugated GO. A high-resolution TEM image, as shown in Figure 2A, clearly shows that a single SK-BR-3 cancer cell is conjugated inside of the GO sheet. To find out the biocompatibility of S6 RNA aptamer-conjugated GO, 6.4×10^4 cells/mL of cancer cells were incubated with S6 RNA aptamer-conjugated GO for different time intervals until 24 h. After that, the cell viability was measured using an MTT test.[6,7] Figure 2F clearly shows that even after 24 h of incubation with SK-BR-3 cancer cells, 98% cell viability was observed. Next, to explore the cytotoxicity of S6 RNA aptamer-conjugated GO against normal living cells, we performed a cytotoxicity test using human skin cell line, HaCaT keratinocytes. As shown in Figure 2G, 98% cell viability was observed even after 24 h of

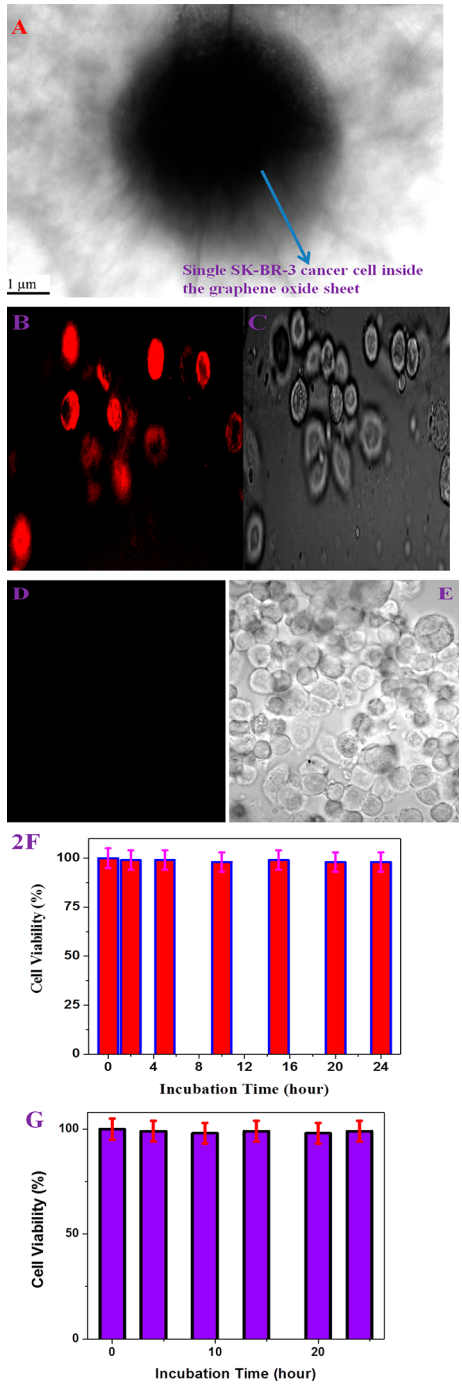

Figure 2. (A) TEM image shows that a single SK-BR-3 cancer cell is conjugated inside of the GO sheet. (B) Two-photon luminescence image of S6 RNA aptamer-conjugated GO attached to SK-BR-3 breast cancer cells. We used 1100 nm light as the excitation source. (C) Bright-field image of the same cells. (D) Two-photon luminescence image of of S6 RNA aptamer-conjugated GO with MDA-MB-231 breast cancer cells. Our result clearly shows that S6 RNA aptamer-attached hybrid GO does not bind with the MDA-MB-231 breast cancer cell. (E) Bright-field image of the same cells. (F) Plot demonstrates the biocompatibility of S6 RNA aptamer-conjugated GO against SK-BR-3 breast cancer cells. Even after 24 h of incubation, we observed about 98% cell viability. (G) Plot shows the biocompatibility of S6 RNA aptamer-conjugated GO against human skin cell line, HaCaT keratinocytes cells. Even after 24 h of incubation, we observed about 99% cell viability.

dx.doi.org/10.1021/jz5009856 | J. Phys. Chem. Lett. 2014, 5, 2150−2154

incubation. All the above-reported cytotoxicity results clearly show very good biocompatibility of S6 RNA aptamer-conjugated GO prepared in our group. Figure 2B,C shows the two-photon luminescence image of SK-BR-3 cells using S6 RNA aptamer-conjugated GO, which indicates that aptamer-conjugated GO can be used for very bright two-photon imaging of cancer cells.

Next, to find out whether S6 RNA aptamer-conjugated GO-based two-photon luminescence is selective for SK-BR-3 cell imaging, we incubated S6 RNA aptamer-conjugated GO with 8.4×10^4 cells/mL of nontargeted MDA-MB-231 breast cancer cells for 30 min. After that, unconjugated MDA-MB-231 breast cancer cells were separated using centrifugation followed by washing with buffer three times. Two-photon fluorescence images, as shown in Figure 2D,E, clearly show that nontargeted MDA-MB-231 breast cancer cells do not bind with S6 RNA aptamer-conjugated GO. The above data clearly show that S6 RNA aptamer-conjugated GO-based two-photon luminescence is highly selective for SK-BR-3 breast cancer tumor imaging.

In conclusion, in this Letter, we have reported S6 RNA aptamer-conjugated GO as a two-photon luminescence platform for targeted SK-BR-3 breast cancer cell imaging. Reported experimental results indicate extremely high two-photon absorption cross-section (46890 GM) from S6 RNA aptamer-conjugated GO. Our data show that two-photon luminescence signal remains unchanged, even after 2 h of illumination. Our reported data indicate that S6 RNA aptamer-conjugated GO-based two-photon luminescence platform can be used for selective imaging of breast cancer cells, in second biological transparency windows. Experimental results with nontargeted MDA-MB-231 breast cancer cells indicates that S6 RNA aptamer-conjugated GO-based two-photon luminescence is highly selective for SK-BR-3 breast cancer tumor imaging. After proper engineering design, aptamer-modified GO can be a good candidate for two-photon cancer imaging in clinical settings.

MATERIALS AND EXPERIMENTS

We obtained all chemicals, including graphite, $KMnO_4$, sodium borohydride, sodium citrate, and nitric acid from Sigma-Aldrich and Fisher Scientific. We purchased SK-BR-3 and MDA-MB-231 breast cancer cell lines, growth media to grow cancer cells, buffered saline, trypsin, and fetal bovine serum from the American Type Culture Collection (ATCC, Rockville, MD).

GO was synthesized using a modified Hummers method from graphite exfoliation,[24] as we and others have reported earlier.[25−30] For targeted two-photon imaging of SK-BR-3 cancer cells, we modified GO with S6 RNA aptamer. At first, GO was coated by thiolated HS-PEG. After PEGylation, NH-modified S6 RNA aptamers were attached with acid chloride-functionalized GO.

Breast cancer cells were grown according to the ATCC procedure and also using our reported method.[6,7] We grew cells in a 5% CO_2 incubator at 37 °C using ATCC medium supplemented with 10% premium fetal bovine serum (FBS) and antibiotics (10 IU/mL penicillin G and streptomycin) in 75 cm^2 tissue culture flasks. The HaCaT cells were also grown in Dulbecco's Modified Eagle's Medicum (DMEM), as instructed by ATCC. Different numbers of breast cancer cells were then spiked with aptamer-attached GO. After that, the mixtures were incubated for different times.

For two-photon imaging at 1100 nm light, we used a Nikon multiphoton microscope (FV1000MPE) as we reported earlier.[11] We used an 80 MHz Ti-sapphire laser as an excitation source with 100 fs pulse width and 80 MHz repetition rate. 1100 nm light in second biological transparency windows was generated using an optical parametric amplifier.

AUTHOR INFORMATION

Corresponding Author

*E-mail: paresh.c.ray@jsums.edu; Fax: +16019793674.

Notes

The authors declare no competing financial interest.

ACKNOWLEDGMENTS

P.C.R. thanks NSF-PREM, Grant # DMR-1205194, for their generous funding.

REFERENCES

(1) Zamboni, W. C.; Torchilin, V.; Patri, A. K.; Hrkach, J.; Stern, S. Best Practices in Cancer Nanotechnology: Perspective from NCI Nanotechnology Alliance. *Clin. Cancer Res.* **2012**, *18*, 3229−3241.

(2) Van Denderen, B. J. W.; Thompson, E. W. Cancer: The to and fro of Tumour Spread. *Nature* **2013**, *493*, 487−488.

(3) Yu, M.; Bardia, A.; Wittner, B. S.; Stott, S. L.; Smas, M. E.; Ting, D. T.; Isakoff, S. J.; Ciciliano, J. C.; Wells, M. N.; Shah, A. M.; et al. Circulating Breast Tumor Cells Exhibit Dynamic Changes in Epithelial and Mesenchymal Composition. *Science* **2013**, *339*, 580−584.

(4) Advancing the Global Fight Against Cancer. http://www.cancer.org/aboutus/globalhealth, (accessed April 12, 2014).

(5) Dreaden, E. C.; Alkilany, A. M.; Huang, X.; Murphy, C. J.; El-Sayed, M. A. The Golden Age: Gold Nanoparticles for Biomedicine. *Chem. Soc. Rev.* **2012**, *41*, 2740−2779.

(6) Lu, W.; Singh, A. K.; Khan, S. A.; Senapati, D.; Yu, H.; Ray, P. C. Gold Nano-Popcorn-Based Targeted Diagnosis, Nanotherapy Treatment, and *In Situ* Monitoring of Photothermal Destruction Response of Prostate Cancer Cells Using Surface-Enhanced Raman Spectroscopy. *J. Am. Chem. Soc.* **2010**, *132*, 18103−18114.

(7) Fan, Z.; Shelton, M.; Singh, A. K.; Senapati, D.; Khan, S. A.; Ray, P. C. Multifunctional Plasmonic Shell−Magnetic Core Nanoparticles for Targeted Diagnostics, Isolation, and Photothermal Destruction of Tumor Cells. *ACS Nano* **2012**, *6*, 1065−1073.

(8) Bardhan, R.; Lal, S.; Joshi, A.; Halas, N. J. Theranostic Nanoshells: From Probe Design to Imaging and Treatment of Cancer. *Acc. Chem. Res.* **2011**, *44*, 936−946.

(9) Lu, W.; Arumugam, S. R.; Senapati, D.; Singh, A. K.; Arbneshi, T.; Khan, S. A.; Yu, H.; Ray, P. C. Multifunctional Oval Shape Gold Nanoparticle Based Selective Detection of Breast Cancer Cells Using Simple Colorimetric and Highly Sensitive Two-Photon Scattering Assay. *ACS Nano* **2010**, *4*, 1739−1749.

(10) Huang, X.; El-Sayed, I. H.; Qian, W.; El-Sayed, M. A. Cancer Cell Imaging and Photothermal Therapy in the Near-Infrared Region by Using Gold Nanorods. *J. Am. Chem. Soc.* **2006**, *128*, 2115−2120.

(11) Demeritte, T.; Fan, Z.; Sinha, S. S.; Duan, J.; Pachter, R.; Ray, P. C. Gold Nanocage Assembly for Selective Second Harmonic Generation Imaging of Cancer Cell. *Chem.—Eur. J.* **2014**, *20*, 1017−1022.

(12) Truong, T. V.; Supatto, W.; Koos, D. S.; Choi, J. M.; Fraser, S. E. Deep and Fast Live Imaging With Two-Photon Scanned Light-Sheet Microscopy. *Nat. Methods.* **2011**, *8*, 757−760.

(13) Smith, A. M.; Mancini, M. C.; Nie, S. Bioimaging: Second Window for *in Vivo* Imaging. *Nat. Nanotechnol.* **2009**, *4*, 710−711.

(14) Planchon, T. A.; Gao, L.; Milkie, D. E.; Davidson, M. W.; Galbraith, J. A.; Gainbraith, C. G.; Betzig, E. Rapid Three-Dimensional Isotropic Imaging of Living Cells Using Bessel Beam Plane Illumination. *Nat. Methods* **2011**, *8*, 417−423.

(15) Huschka, R.; Neumann, O.; Barhoumi, A.; Halas, N. J. Visualizing Light-Triggered Release of Molecules Inside Living Cells. *Nano Lett.* **2010**, *10*, 4117−4122.

(16) Maestro, L. M.; Rodríguez, E. M.; Rodríguez, F. S.; Cruz, M. C. I.; Juarranz, A.; Naccache, R.; Vetrone, F.; Jaque, D.; Capobianco, J. A.; Solé, J. G. CdSe Quantum Dots for Two-Photon Fluorescence Thermal Imaging. *Nano Lett.* **2010**, *10*, 5109−5115.
(17) Park, J. H.; Gu, L.; von Maltzahn, G.; Ruoslahti, E.; Bhatia, S. N.; Sailor, M. J. Biodegradable Luminescent Porous Silicon Nanoparticles for In Vivo Applications. *Nat. Mater.* **2009**, *8*, 331−336.
(18) Park, J. Anchored Proteinase-Targetable Optomagnetic Nanoprobes for Molecular Imaging of Invasive Cancer Cells. *Angew. Chem., Int. Ed.* **2012**, *51*, 945−948.
(19) Chen, Z.; Hong, G.; Wang, H.; Welsher, K.; Tabakman, S. M.; Sherlock, S. P.; Robinson, J. T.; Liang, Y.; Dai, H. Graphite-Coated Magnetic Nanoparticle Microarray for Few-Cells Enrichment and Detection. *ACS Nano* **2012**, *6*, 1094−1101.
(20) Larson, D. E.; Zipfel, W. R.; Williams, R. M.; Clark, S. W.; Bruchez, M. P.; Wise, F. W.; Webb, W. W. Water-Soluble Quantum Dots for Multiphoton Fluorescence Imaging in Vivo. *Science* **2003**, *300*, 1434−1436.
(21) Robinson, J. T.; Tabakman, S. M.; Liang, Y.; Wang, H.; Casalongue, S. H.; Vinh, D.; Dai, H. Ultrasmall Reduced Graphene Oxide with High Near-Infrared Absorbance for Photothermal Therapy. *J. Am. Chem. Soc.* **2011**, *133*, 6825−6831.
(22) Liu, Z.; Robinson, J. T.; Sun, X.; Dai, H.; Wang, Y.; Li, Z.; Hu, D.; Lin, C.-T.; Li, J.; Lin, Y. Aptamer/Graphene Oxide Nanocomplex for *in Situ* Molecular Probing in Living Cells. *J. Am. Chem. Soc.* **2010**, *132*, 9274−9276.
(23) Novoselov, K. S.; Fal, V. I.; Colombo, L.; Gellert, P. R.; Schwab, M. G.; Kim, K. A. Roadmap for Graphene. *Nature* **2012**, *490*, 192−200.
(24) Hummers, W. S.; Offeman, R. E. Preparation of Graphitic Oxide. *J. Am. Chem. Soc.* **1958**, *80*, 1339−1344.
(25) Lightcap, I. V.; Kamat, P. V. Graphitic Design: Prospects of Graphene-Based Nanocomposites for Solar Energy Conversion, Storage, and Sensing. *Acc. Chem. Res.* **2013**, *46*, 2235−2243.
(26) Kamat, P. V. Graphene-Based Nanoarchitectures. Anchoring Semiconductor and Metal Nanoparticles on a Two-Dimensional Carbon Support. *J. Phys. Chem. Lett.* **2010**, *1*, 520−527.
(27) Fan, Z.; Kanchanapally, R.; Ray, P. C. Hybrid Graphene Oxide Based Ultrasensitive SERS Probe for Label-Free Biosensing. *J. Phys. Chem. Lett.* **2013**, *4*, 3813−3818.
(28) Kanchanapally, R.; Sinha, S. S.; Fan, Z.; Dubey, M.; Zakar, E.; Ray, P. C. Graphene Oxide−Gold Nanocage Hybrid Platform for Trace Level Identification of Nitro Explosives Using a Raman Fingerprint. *J. Phys. Chem. C* **2014**, *4*, 7070−7075.
(29) Loh, K. P.; Bao, Q.; Eda, G.; Chhowalla, M. Graphene Oxide as a Chemically Tunable Platform for Optical Applications. *Nat. Chem.* **2010**, *2*, 1015−1024.
(30) Kozawa, D.; Miyauchi, Y.; Mouri, S.; Matsuda, K. Exploring the Origin of Blue and Ultraviolet Fluorescence in Graphene Oxide. *J. Phys. Chem. Lett.* **2013**, *4*, 2035−204.
(31) Chien, C. T.; Li, S. S.; Lai, W. J.; Yeh, Y. C.; Chen, H. A.; Chen, I. S.; Chen, L. C.; Chen, K. H.; Nemoto, T.; Isoda, S. Tunable Photoluminescence from Graphene Oxide. *Angew. Chem., Int. Ed.* **2012**, *51*, 6662−6666.
(32) Shang, J.; Ma, L.; Li, J.; Ai, W.; Yu, T.; Gurzadyan, G. G. The Origin of Fluorescence from Graphene Oxide. *Sci. Rep.* **2012**, *2*, 792.
(33) Kim, J.; Cote, L. J.; Kim, F.; Huang, J. Visualizing Graphene Based Sheets by Fluorescence Quenching Microscopy. *J. Am. Chem. Soc.* **2010**, *132*, 260−267.
(34) Exarhos, A. L.; Turk, M. E.; Kikkawa, J. M. Ultrafast Spectral Migration of Photoluminescence in Graphene Oxide. *Nano Lett.* **2013**, *13*, 344−349.
(35) Cushing, S. K.; Li, M.; Huang, F.; Wu, N. Origin of Strong Excitation Wavelength Dependent Fluorescence of Graphene Oxide. *ACS Nano* **2014**, *8*, 1002−1013.
(36) Zhu, X.; Su, H. B. Exciton Characteristics in Graphene Epoxide. *ACS Nano* **2014**, *8*, 1284−1289.
(37) Kumar, P.; Bernardi, M.; Grossman, J. The Impact of Functionalization on the Stability, Work Function, and Photoluminescence of Reduced Graphene Oxide. *ACS Nano* **2013**, *7*, 1638−1645.
(38) Liu, Z.-B.; Zhao, X.; Zhang, X.-L.; Yan, X.-Q.; Wu, Y.-P.; Chen, Y.-S.; Tian, J.-G. Ultrafast Dynamics and Nonlinear Optical Responses from sp^2- and sp^3-Hybridized Domains in Graphene Oxide. *J. Phys. Chem. Lett.* **2011**, *2*, 1972−1977.
(39) Dimiev, A.; Alemany, L.; Tour, J. Graphene Oxide. Origin of Acidity, Its Instability in Water, and a New Dynamic Structural Model. *ACS Nano* **2013**, *7*, 576−588.
(40) Liu, Q.; Guo, B.; Rao, Z.; Zhang, B.; Ru, J. Strong Two-Photon-Induced Fluorescence from Photostable, Biocompatible Nitrogen-Doped Graphene Quantum Dots for Cellular and Deep-Tissue Imaging. *Nano Lett.* **2013**, *13*, 2436−2441.
(41) Cao, L.; Meziani, M. J.; Sahu, S.; Sun, Y.-P. Photoluminiscence Properties of Graphene versus Other Carbon Nanomaterials. *Acc. Chem. Res.* **2013**, *46*, 171−180.
(42) Konkena, B.; Vasudevan, S. Spectral Migration of Fluorescence in Graphene Oxide Aqueous Dispersions: Evidence for Excited-State Proton Transfer. *J. Phys. Chem. Lett.* **2014**, *5*, 1−7.
(43) Mei, Q.; Zhang, Z. Photoluminescent Graphene Oxide Ink to Print Sensors onto Microporous Membranes for Versatile Visualization Bioassays. *Angew. Chem., Int. Ed.* **2012**, *51*, 5602−5606.
(44) Mei, Q.; Jiang, C.; Guan, G.; Zhnag, K.; Liu, B.; Liu, R.; Zhang, Z. Fluorescent Graphene Oxide Logic Gates for Discrimination of Iron (3+) and Iron (2+) in Living Cells by Imaging. *Chem. Commun.* **2012**, *48*, 7468−7470.
(45) King, S. H.; Huh, Y. M.; Kim, S.; Lee, D.-K. Isolation of RNA Aptamers Targeting HER-2-Overexpressing Breast Cancer Cells Using Cell-SELEX. *Bull. Korean Chem. Soc.* **2009**, *30*, 1827−1831.